Desalination and Water Treatment
www.deswater.com
doi: 10.1080/19443994.2015.1041052

57 (2016) 10790–10801
May

Taylor & Francis
Taylor & Francis Group

Surface modification of TiO_2 nanotube arrays with metal copper particle for high efficient photocatalytic reduction of Cr(VI)

Mengyao Wu, Tigang Duan, Ye Chen*, Qing Wen*, Yuyang Wang, Hongmei Xin

Key Laboratory of Superlight Material and Surface Technology of Ministry of Education, College of Materials Science and Chemical Engineering, Harbin Engineering University, Harbin 150001, China, Tel. +86 13845117524; email: wumengyao102109@sina.com (M. Wu), Tel. +86 15045648001; email: duantigang@hrbeu.edu.cn (T. Duan), Tel. +86 13059004260; email: chenye@hrbeu.edu.cn (Y. Chen), Tel. +86 13039978811; email: wenqing@hrbeu.edu.cn (Q. Wen), Tel. +86 18645063500; email: wangyuyanglover@163.com (Y. Wang), Tel. +86 13115502691; email: xinhongmei@hrbeu.edu.cn (H. Xin)

Received 17 July 2014; Accepted 8 April 2015

ABSTRACT

Highly ordered TiO_2 nanotube arrays (NTs) have been widely used for photocatalysis application. In this study, to further improve the photocatalysis activity of TiO_2 NTs, Cu/TiO_2 NTs were prepared through an anodic oxidation and impregnation–reduction method. The morphology and crystalline phase of the pure TiO_2 NTs and Cu/TiO_2 NTs were characterized by SEM and X-ray diffraction. The photocatalytic performance of Cu/TiO_2 NTs was evaluated by photocatalytic reduction of Cr(VI) under UV light. The rate constant of photocatalytic reduction of Cr(VI) on $Cu_{0.01}/TiO_2$ NTs which had the optimal Cu loading content was 9.5 times higher than that on unmodified TiO_2 NTs. And the experiment results of different initial concentration of Cr(VI) and pH demonstrated that they greatly influenced the removal efficiency of Cr(VI). The photoelectric properties of TiO_2 NTs with Cu particle loading were investigated by photoelectrochemical characterization, including photocurrent response, open-circuit voltage, electro-chemical impedance spectroscopy Nynquist plots, and Mott–Schottky plots. The enhancement of the photocatalytic performance of Cu/TiO_2 NTs indicated that the electrons could transfer faster and be utilized more easily due to the formation of Schottky barrier on the interface of Cu and TiO_2. The detailed electrons transfer mechanism of Cu/TiO_2 NTs was proposed.

Keywords: Cu/TiO_2 NTs; Cr(VI); Photocatalytic reduction

1. Introduction

Hexavalent chromium is a common universal metal pollutant in natural waters, which is seriously harmful for human health. The principal source of chromium is from industrial processes, such as alloying, metal electroplating, and the application of chemistry [1]. Due to its high toxicity and strong carcinogenicity, the Cr(VI) level for drinking water is below 0.05 mg L^{-1} according to the World Health Organization [2]. However, Cr(III) is less toxic than Cr(VI) and can be readily precipitated as $Cr(OH)_3$ in alkaline or neutral solutions [3–5]. Recently, the semiconductor photocatalysis technology for reduction of Cr(VI) to less harmful Cr(III) has obtained considerable attention because of its high effectiveness, chemical stability, and low toxicity [6–12]. The use of TiO_2

*Corresponding authors.

has been most frequently among all semiconductor materials [13–15].

However, there are two major factors limiting the application of TiO_2 in the field of photocatalysis due to TiO_2 intrinsic defects [16–18]. The first factor is the high band gap of TiO_2 (3.0–3.2 eV) which indicates that TiO_2 can be excited by UV light that is only 3% of the solar spectrum [19]. To extend the absorption range of the solar spectrum, researchers make efforts on combination with narrow-band-gap semiconductors, for example some chalcogenide semiconductor such as PbS [20,21], CdS [22–24] and Bi_2S_3 [25] or some metallic oxide such as Bi_2O_3 [26], Fe_2O_3 [27,28], and Cu_2O [29–31]. The second factor is low electron transfer rate on the interface and high recombination of photogenerated electrons and holes pairs. To suppress the electrons and holes recombination and enhance the charge separation efficiency [32], some noble metals have been explored to be in contact with TiO_2, such as Ag [33,34], Pt [35], and Au [36]. The obtained results suggest that electrons can transfer from TiO_2 to the metal particles when the Fermi level of metals is more negative than the conduction band of TiO_2. A Schottky barrier can form at the metal–semiconductor contacting region, which can act as electron scavengers to avoid effectively the electron–hole recombination [37]. Although TiO_2 modified by noble metals has high photocatalytic activity, the high cost restricts their practical application in the field of wastewater treatment. Therefore, TiO_2 modified by non-precious metal for improving its photocatalytic activity has a promising future in practical application.

Some authors have reported effective TiO_2 modified by non-precious transition metals, such as Fe, Zn, Cu, Ni, and so on. Xiao et al. [38] reported that the photocurrent response of TiO_2 nanotube arrays (NTs) electrodes loaded with Zn nanoparticles has increased to 50% under high-pressure mercury lamp illumination when compared with pure TiO_2 NTs. The Fe/TiO_2 nanocomposites can retain both the dechlorination and degradation of organic pollutants under UV light since Fe has a strong reducing power [39]. Liu et al. [40] reported that Ni-loaded TiO_2 nanoparticles showed better photocatalytic activity than that of TiO_2 on the degradation of methyl orange. Copper is a promising metal which has more negative Fermi level (Fermi level of Cu is −4.7 eV, Fe is −4.5 eV, Zn is −4.3 eV vs. vacuum level) and good electronic conductivity only after Ag. Kim et al. [41] reported that the catalyst of Cu-modified TiO_2 powder showed the highest photocatalytic activity for cyanide conversion than Ni, Co, and Ag. And Cu is a relatively abundant and cheap metal when compared with other transition metals [42]. Moreover, Cu has stable property which is favorable to improve the service life of the catalyst. The low cost and good electron transfer ability make copper a better choice for modification of TiO_2.

The nanostructure materials have attracted great interest as most promising architectures due to the special architecture, high charge transport rate, and significant light-harvest property [43]. Self-organized anodic titania NTs have been extensively regarded as an efficient nanostructure to improve the photocatalytic activity because of their large specific surface area, highly ordered structure, and outstanding photocatalytic properties. Moreover, TiO_2 NTs can be easily operated and recycled in the practical application comparing with the TiO_2 powders which need filtration after a period of photocatalytic reaction [44]. However, few works focus on the Cu-modified TiO_2 TNs catalyst by now.

In this paper, highly ordered TiO_2 TNs were prepared by anodization, followed by annealing treatment. Then, the copper particle coating was fabricated by an impregnation–reduction method for reduction of the precursor Cu^{2+} to Cu using UV irradiation on TiO_2 TNs. The Cu/TiO_2 NTs were characterized by scanning electrons microscopy (SEM) and X-ray diffraction (XRD). And then, Cr(VI) was selected as the typical heavy metal ions and degraded for photocatalytic reduction with varied loading content Cu/TiO_2 NTs under UV light. The photoelectrochemical behaviors of Cu/TiO_2 NTs were evaluated by photocurrent response, open-circuit potential (OCP), electro-chemical impedance spectroscopy (EIS), and Mott–Schottky analysis. Furthermore, the mechanism of the photocatalytic on Cu/TiO_2 NTs was studied.

2. Experimental

2.1. Preparation of Cu/TiO_2 NTs

The Ti sheets (0.5 mm thickness, 99.6% purity, Japan) were used as the substrate for highly ordered TiO_2 NTs electrochemical anodic oxidation. The chemical reagents were all of analytical grade and purchased from the Tianjin Kermel Chemical Company, China. Prior to the anodization, Ti sheets went through mechanical polishing, degreasing in a 10% NaOH solution at 85˚C for 1 h, and etching in a 10% oxalic acid solution at 85˚C for 2 h. And then pretreated Ti sheets were cleaned using distilled water. The electrochemical anodization process was performed in a two-electrode system with Ti sheets as both the working electrode and the counter electrode under magnetic agitation at room temperature. The electrolyte was the mixed ethylene glycol solution of 0.2 mol L^{-1} NH_4F and 3 vol% H_2O. The anodization consisted of two periods under a 60 V anodic potential. The Ti sheet was first anodizated

for 0.5 h and ultrasonically cleaned in 2 vol% hydrochloric acid for 10 min aimed at removing irregular initial TiO_2 nanotube layer. The second period is constant for 1 h and then ultrasonically cleaned with ethanol solution and dried in the air. The amorphous TiO_2 NTs were annealed in an oven at 500 ℃ for 1 h in the air atmosphere.

The Cu/TiO_2 NTs were prepared by an impregnation–reduction method [45]. Two steps are as follows: (1) To prepare Cu/TiO_2 NTs with different Cu loading content, the TiO_2 NTs were impregnated in 0.005, 0.01, 0.03, and 0.05 mol L^{-1} $CuSO_4$ as a Cu precursor for 6 h at vacuum condition in order to make more Cu^{2+} enter the interior of the tube, and then dried in the air for 1 h. The Cu_x/TiO_2 NTs refer to the TiO_2 NTs impregnating in x mol L^{-1} $CuSO_4$ solution. (2) The samples were irradiated by a 80 W UV light (λ = 365 nm) in methanol solution which is regarded as a hole scavenger for 6 h sufficient to induce photocatalytic reduction of Cu^{2+} ions to metallic Cu particles. Finally, the obtained samples were washed gently with distilled water and dried naturally in the air atmosphere.

2.2. Characterization and photoelectrochemical measurements

The morphological investigation of Cu/TiO_2 NTs was scanned by scanning electron microscope (INSPECT S50, MAKE FEI). XRD (Rigaku D/Max2500) was performed with a Cu Kα radiation at 40 kV and 150 mA to obtain the crystalline patterns of samples.

The photoelectrochemical experiment was performed in a conventional three-electrode system recorded by an electrochemical workstation (SP-240, BioLogic Science Instruments, France). The prepared Cu/TiO_2 electrodes served as the working electrode with a test area of 1×1 cm^2. A platinum sheet (2×2 cm^2) and saturated calomel electrode (SCE) were used as a counter and a reference electrode, respectively. The electrolyte was 0.25 mol L^{-1} Na_2SO_4 solution and an 8 W UV lamp was used as the UV light source (λ = 365 m). EIS was conducted in a range of 10^4–10^{-1} Hz at OCP with an amplitude signal of 5 mV in the dark and under UV illumination. Mott–Schottky plots for testing the capacitance behavior were acquired under UV illumination ranged from −0.1 to 1.0 V with potential steps of 5 mV at frequency of 1 kHz.

2.3. Photocatalytic reduction of Cr(VI) under UV light

The photocatalytic activity was evaluated by the reduction of Cr(VI) under UV illumination using an 80 W UV lamp (λ = 365 m). The working electrode area is 2×2 cm^2. The reduction experiments were performed in 100 mL containing $K_2Cr_2O_7$ aqueous solution. The pH was adjusted using H_2SO_4 solution. The Cr(VI) concentrations were measured by UV/vis spectrophotometer using the diphenylcarbazide method at 540 nm.

3. Result and discussion

3.1. Characterization of TiO_2 NTs and Cu/TiO_2 NTs

From the SEM image of TiO_2 NTs (Fig. 1(a)), the pure TiO_2 NTs grow vertically on the titanium

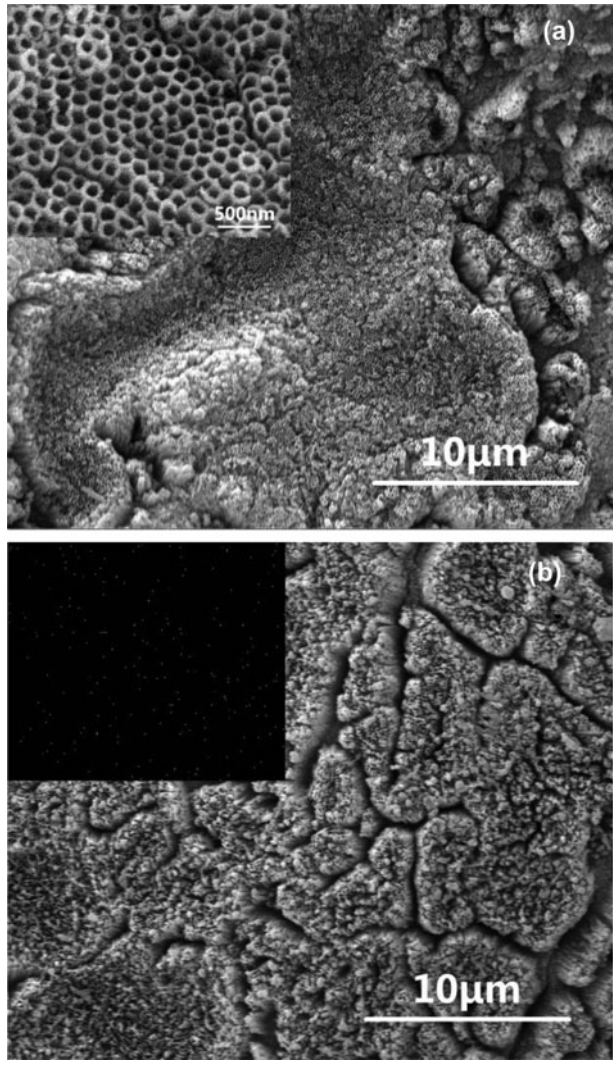

Fig. 1. The SEM images of (a) TiO_2 NTs, insert: higher magnification and (b) $Cu_{0.01}/TiO_2$ NTs, insert: EDS-mapping of $Cu_{0.01}/TiO_2$ NTs.

substrate and the nanotubes were highly ordered, uniform with an average diameter of approximately 130 nm and a wall thickness of about 40 nm. After Cu was loaded on the TiO_2 NTs, no obvious change of the morphologies was observed on the top. The Cu/TiO_2 NTs were still with high orientation. And the top was opened without losing their architectures (Fig. 1(b)). The EDS result suggests the atom percentage of Cu element on $Cu_{0.01}/TiO_2$ NTs is 1.5%. X-ray dot-mapping was used for analyzing the distribution of coating elements. From Fig. 1(b) inset, it showed a uniform distribution of Cu on the TiO_2 NTs surface. From the SEM image, the TiO_2 NTs have stable structure with uniform size, high orientation, large particular surface area, which can increase the active sites on the surface of TiO_2 NTs. The BET surface area of TiO_2 NTs is 90 $m^2\ g^{-1}$, which is higher than TiO_2-P25 of 50 $m^2\ g^{-1}$ [46]. N_2 adsorption and desorption isotherms were shown in Fig. S1. At the same time, the uniform distribution of Cu on the TiO_2 NTs can effectively suppress the electrons and holes recombination and improve the charge separation efficiency, which can result in high photocatalytic activity of Cu/TiO_2 NTs.

The morphology of Cu/TiO_2 NTs was further investigated by TEM. The TEM images of TiO_2 NTs and Cu/TiO_2 NTs are shown in Fig. 2. It clearly displays the tubular structure of TiO_2 NTs with open ends in Fig. 2. The diameter of TiO_2 NTs is about 130 nm. Fig. 2(b) shows that some small Cu particles with size of 20–40 nm attached to the walls of TiO_2 NTs. From the electron diffraction (SAED) patterns, several diffraction rings can be indexed to Cu (1 1 1) (2 0 0) (2 2 0) (Fig. 2(b) inset). Fig. 2(c) shows that lattice spacing of 3.50 Å corresponds to the (1 0 1) plane of anatase TiO_2.

The crystal structures of the pure TiO_2 NTs and $Cu_{0.01}/TiO_2$ NTs samples were compared by XRD measurement, as shown in Fig. 3. The diagrams display the diffraction peaks which are corresponding to the Ti substrate, anatase, and metallic copper (noted T, A and C, respectively). The peaks of metal Ti phase resulted from the Ti substrate of samples. When the samples were annealed at 500°C for 1 h, the peaks of TiO_2 were all ascribed to the anatase phase without the rutile phase. In fact, the well-crystallized anatase TiO_2 phase shows higher catalytic activity and easily photo-generates electron–hole pairs due to the instability under UV light. After Cu loaded on the TiO_2 NTs, three peaks at 2θ = 43.3°, 50.4°, and 74.1° were clearly exhibited which correspond to the characteristic peaks of metallic Cu (1 1 1) (2 0 0) (2 2 0) [47]. Also, the diffraction peaks of the TiO_2 NTs were almost

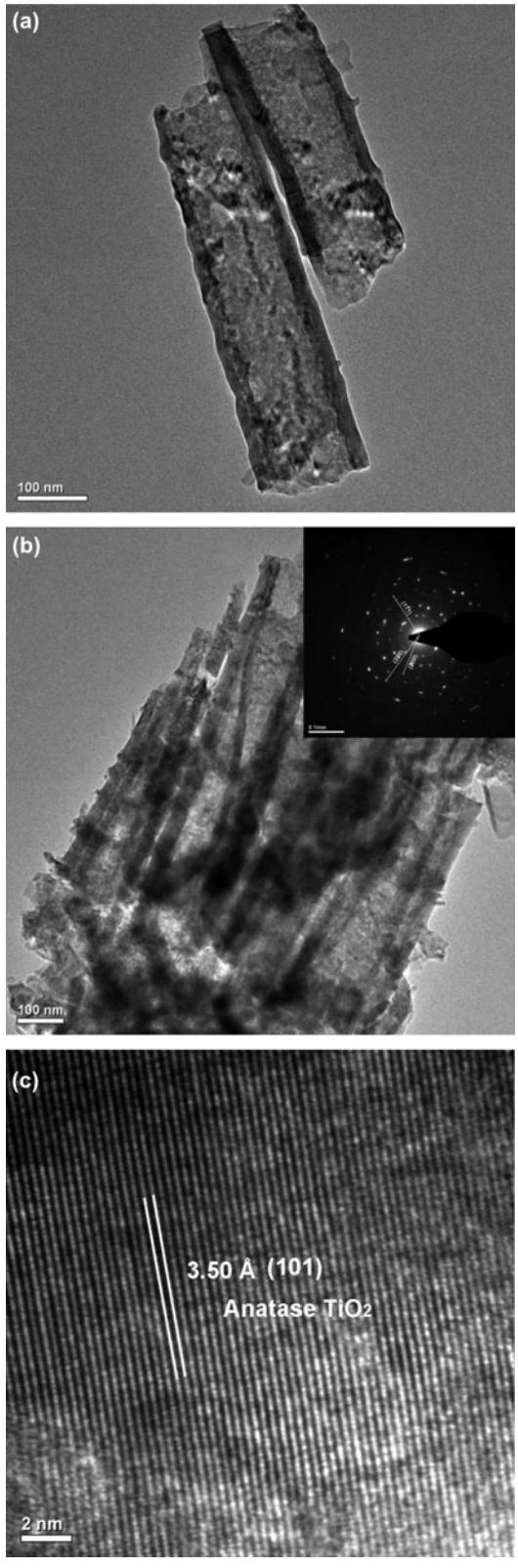

Fig. 2. TEM images of (a) TiO_2 NTs and (b) Cu/TiO_2 NTs; HRTEM of (c) TiO_2 NTs.

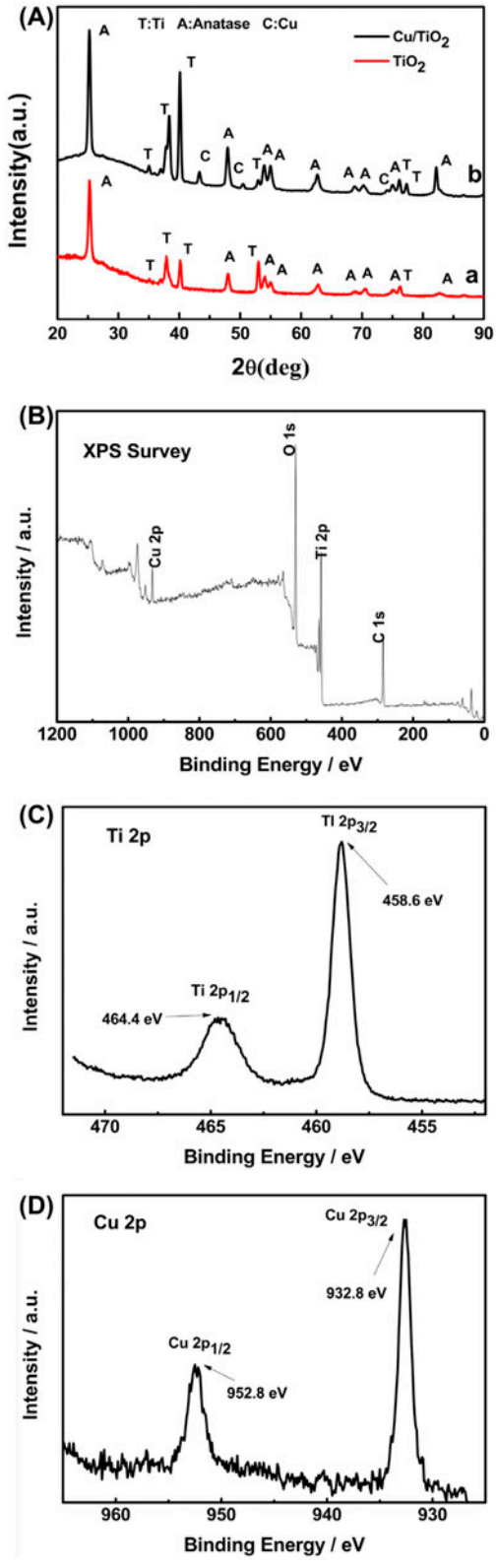

Fig. 3. (A) XRD patterns of TiO_2 NTs and $Cu_{0.01}/TiO_2$ NTs; XPS spectra of $Cu_{0.01}/TiO_2$ NTs, (B) a survey scan, (C) Cu 2p, and (D) Ti 2p.

unchanged with on observable shift after the Cu photo-deposition, indicating that Cu was not incorporated into the lattice and was physically attached on the surface of TiO_2 NTs. The morphology and crystalline phase of Cu/TiO_2 NTs are both advantageous for efficient photocatalytic activity.

In addition, the XPS spectra of $Cu_{0.01}/TiO_2$ NTs are presented in Fig. 3(B). In particular, Ti 2p (Fig. 3(C)) and Cu 2p (Fig. 3(D)) are also shown. In the Ti 2p spectrum, the peaks located at 458.6 and 464.4 eV correspond to Ti $2p_{3/2}$ and Ti $2p_{1/2}$. And the splitting of 5.8 eV between the two peaks indicates that Ti^{4+} exists in the TiO_2 NTs [48]. In the Cu 2p spectrum, two peaks at the binding energies of 932.8 and 952.8 eV were observed, respectively, corresponding to Cu $2p_{3/2}$ and Cu $2p_{1/2}$. The satellite peak at about 934.3 eV characterizing for Cu^{2+} could not be seen, indicating that the absence of CuO. The XPS results further demonstrate that the sample contains pure Cu(0) rather than Cu^{2+} [49,50].

3.2. Photocatalytic reduction of Cr(VI)

3.2.1. Effect of different Cu loading content on photocatalytic property

The photocatalytic activity of different loading content Cu/TiO_2 NTs was investigated by photocatalytic reduction efficiency of Cr(VI). The effect of different Cu loading content on photocatalytic reduction of Cr(VI) under UV light (365 nm) is shown in Fig. 4. The removals of Cr(VI) on Cu/TiO_2 NTs were much higher than that of unmodified TiO_2 NTs, indicating that the Cu/TiO_2 NTs exhibit higher photocatalytic activities, which was owed to the fast electrons and holes separation rate and the rapid charge transfer from the conduction band to Cu particles. The fastest removal of Cr(VI) on $Cu_{0.01}/TiO_2$ NTs was 99% while that on unmodified TiO_2 NTs was 37% at pH 2.5 for the initial Cr(VI) concentration of 10 mg L^{-1}. The removal of Cr(VI) had 62% significant enhancement on Cu-modified TiO_2 NTs. Additionally, the photocatalytic activity of different loading content Cu/rutile TiO_2 NTs was also investigated (the rutile TiO_2 NTs were obtained through annealing amorphous TiO_2 NTs at 700°C for 1 h). And the photocatalytic efficiencies were lower than those of Cu/anatase TiO_2 NTs (see Fig. S2 in Supporting Information).

As shown in Fig. 4(B), the kinetic data calculated from the relationship between Cr(VI) concentration and irradiation time are fitted to a rate expression of a pseudo-first-order reaction:

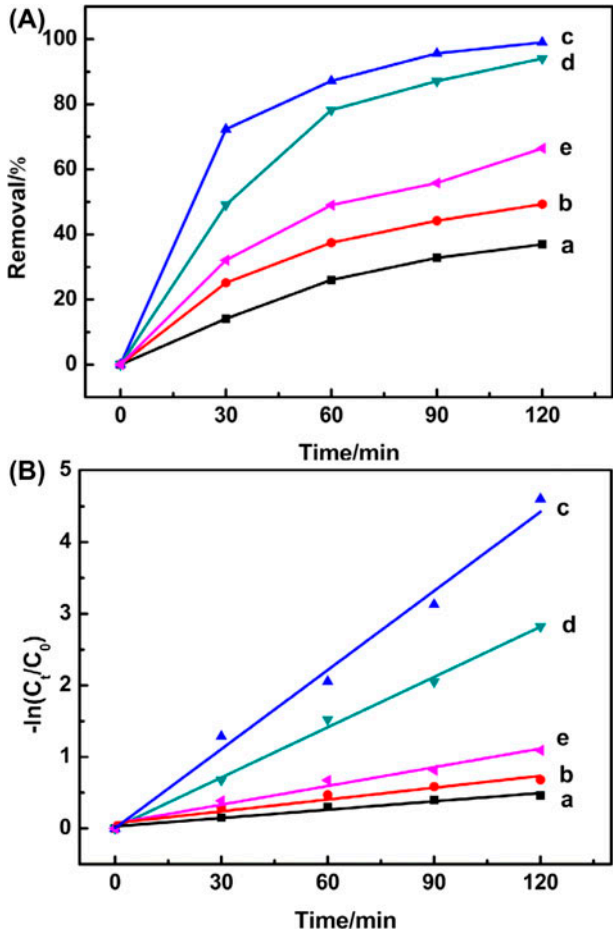

Fig. 4. Effect of different Cu loading on the photocatalytic reduction of Cr(VI) solution (pH 2.5, [Cr(VI)] = 10 mg L^{-1}): (a) TiO_2 NTs, (b) $Cu_{0.005}/TiO_2$ NTs, (c) $Cu_{0.01}/TiO_2$ NTs, (d) $Cu_{0.03}/TiO_2$ NTs, and (e) $Cu_{0.05}/TiO_2$ NTs.

$$\ln(C_t/C_0) = kt \quad (1)$$

where C_t is the concentration of Cr(VI) at time t, C_0 is the initial concentration of Cr(VI), k is the pseudo-first-order rate constant represented by the slope of the fitting line. The fitting results are listed in Table 1.

As illustrated in Table 1 and Fig. 4(B), the rate constant of photocatalytic reduction of Cr(VI) improves with the increasing of the Cu loading content until reaching the highest value, and then has a decrease when continuing to increase the Cu loading content.

Table 1
Rate constants of photocatalytic reduction of Cr(VI)

Sample	Reaction rate, k (min^{-1})	R^2
TiO_2 NTs	0.0039	0.963
$Cu_{0.005}/TiO_2$ NTs	0.0055	0.928
$Cu_{0.01}/TiO_2$ NTs	0.0369	0.986
$Cu_{0.03}/TiO_2$ NTs	0.0234	0.995
$Cu_{0.05}/TiO_2$ NTs	0.0087	0.968

With very small amounts of Cu doping, there will be very few active sites available to conduct a photocatalytic reaction. In contrast, higher Cu doping reduces the surface area, leading to the continuous loss of confinement of the photogenerated charges by the localized regions and thereby decreased photocatalytic activity. The highest rate constant was 0.0369 min^{-1} obtained on $Cu_{0.01}/TiO_2$ NTs, which was 9.5 times higher than that on unmodified TiO_2 NTs (0.0039 min^{-1}). It confirms that the optimal soaking condition is 0.01 mol L^{-1} $CuSO_4$.

To further investigate the effect of different Cu loading on photoelectrochemical property, the linear sweep voltammetry curves carried out under UV-light (365 nm) irradiation for the TiO_2 NTs and Cu/TiO_2 NTs electrodes at a scan rate of 10 mV/s (Fig. 5(A)). When the UV light is open, it means photogenerated hole–electron pairs begin to separate, and the photocurrent gradually increases with the increasing of the applied potential. The photocurrent response of Cu/TiO_2 NTs for different loading content was all higher than that of unmodified TiO_2 NTs. And the maximum photocurrent density of $Cu_{0.01}/TiO_2$ NTs was 0.66 mA cm^{-2} under 2.0 V bias (vs. SCE). The increase in the photocurrent may imply that a Schottky barrier can form on the interface of TiO_2 and Cu, which can play a role for charge rectification like a diode to enhance the separation efficiency of photogenerated electron–hole pairs and accelerate the rate of electron transfer. The mechanism of photogenerated electron–hole transfer will be further detailed.

The corresponding photoconversion efficiency is shown in Fig. 5(B). The photoconversion efficiency means the light energy to chemical energy conversion efficiency, which is evaluated by the following equation [51]:

$$\eta(\%) = [(\text{total power output} - \text{electrical power input})/\text{light power input}] \times 100 = j_p\left(E^0{}_{rev} - |E_{app}|\right)/I_0 \times 100 \quad (2)$$

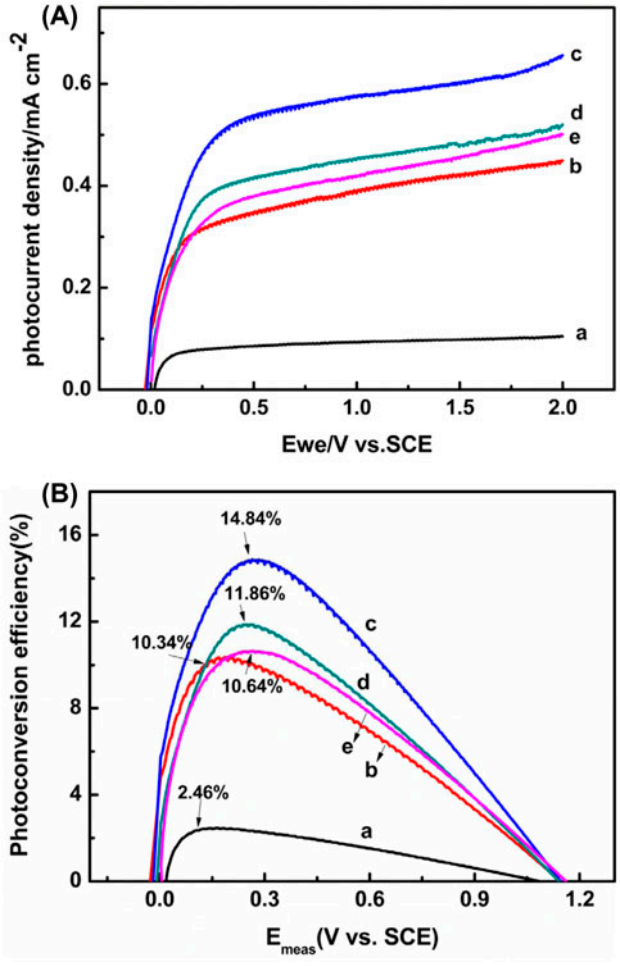

Fig. 5. (A) Photocurrent density of Cu/TiO_2 NTs vs. applied potential curves and (B) the corresponding photoconversion efficiencies: (a) TiO_2 NTs, (b) $Cu_{0.005}/TiO_2$ NTs, (c) $Cu_{0.01}/TiO_2$ NTs, (d) $Cu_{0.03}/TiO_2$ NTs, and (e) $Cu_{0.05}/TiO_2$ NTs.

In above equation, $j_P E^0_{rev}$ stands for the total power output, $j_P|E_{app}|$ stands for the electrical power input, and I_0 is the power density of incident light in mW cm^{-2}. j_p is the photocurrent density in mA cm^{-2}. E^0_{rev} is the standard reversible potential which is 1.23 V (vs. NHE). E_{app} is the applied potential ($E_{app} = E_{meas} - E_{aoc}$, where E_{meas} is the electrode potential (vs. SCE) of the working electrode at which the photocurrent was measured under illumination, and E_{aoc} is the electrode potential (vs. SCE) of the same working electrode at an open circuit under the same conditions).

The maximum photoconversion efficiency for pure TiO_2 NTs, $Cu_{0.005}/TiO_2$ NTs, $Cu_{0.01}/TiO_2$ NTs, $Cu_{0.03}/TiO_2$ NTs, and $Cu_{0.05}/TiO_2$ NTs were 2.46, 10.34, 14.84, 11.86, and 10.64%, respectively. The highest photoconversion efficiency of 14.84% for $Cu_{0.01}/TiO_2$ NTs achieved at 0.3 V vs. SCE was 6 times higher than pure TiO_2 NTs. The increase in photoconversion efficiency for Cu/TiO_2 NTs can be attributed to the high efficiency of charge separation through charge rectification and faster interfacial electrons transfer due to well-dispersed copper particles. However, excessive Cu particles-loaded TiO_2 NTs result in a lower photocurrent. The reason is that excessive Cu particles may decrease the distance of charge carrier space and the recombination centers which could increase recombination. Another reason is that the excess of Cu particles may cover active point on the surface of TiO_2 NTs leading to reduced photocurrent response [52]. In the case of the pure TiO_2 NTs, the recombination can easily happen due to the photogenerated electron–hole pairs. The trend for the photoelectrochemical measurement on TiO_2 NTs of different Cu loading content is corresponding with the removal and the rate constants of photocatalytic reduction of Cr(VI). It further confirms that the $Cu_{0.01}/TiO_2$ NTs have optimal photocatalytic activity, so the following experiment of different effect factors was carried out on $Cu_{0.01}/TiO_2$ NTs.

3.2.2. Effects of initial concentration Cr(VI) and pH on photocatalytic property

The pH and initial concentration Cr(VI) of the solution are important parameters in photocatalytic reduction process. The effect of the initial Cr(VI) concentration on the removal efficiency of Cr(VI) was investigated at pH 2.5 with different initial concentrations of Cr(VI) in the range of 10–40 mg L^{-1}. When the initial concentration of Cr(VI) is low, it is easy for the reduction of Cr(VI) to Cr(III). The maximum reduction efficiency reached 100% for an initial concentration of Cr(VI) of 10 mg L^{-1} at a reaction time of 50 min. Also, the reduction efficiency was only 63.6% at an initial concentration of Cr(VI) of 40 mg L^{-1}. From the kinetic data (Fig. 6(B)), the curves showed a good linear relationship. The rate constants of photocatalytic reduction of Cr(VI) were calculated to be 0.0759, 0.0387, 0.0329, and 0.0166 min^{-1} for initial Cr(VI) concentration 10, 20, 30, and 40 mgL^{-1}, respectively. Therefore, the reduction efficiency of Cr(VI) decreases with the increase in the initial concentration of Cr(VI). Due to the amount of TiO_2 NTs, the active sites are limited. Too many Cr(VI) ions may cover the active sites as adsorbed on the surface of TiO_2 NTs, which could result in the decrease of the reduction efficiency of Cr(VI).

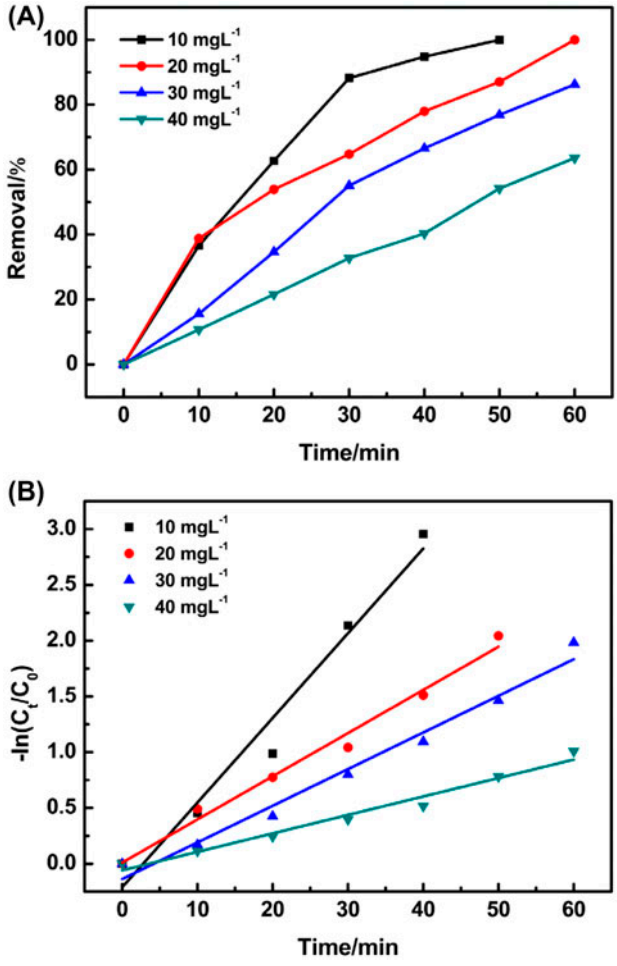

Fig. 6. Effect of the initial Cr(VI) concentration on the photocatalytic reduction of Cr(VI) solution (pH 2.5, ethanol as hole scavenger): (A) Removal efficiency of Cr(VI) and (B) plot of –ln (C_t/C_0) vs. time of Cr(VI).

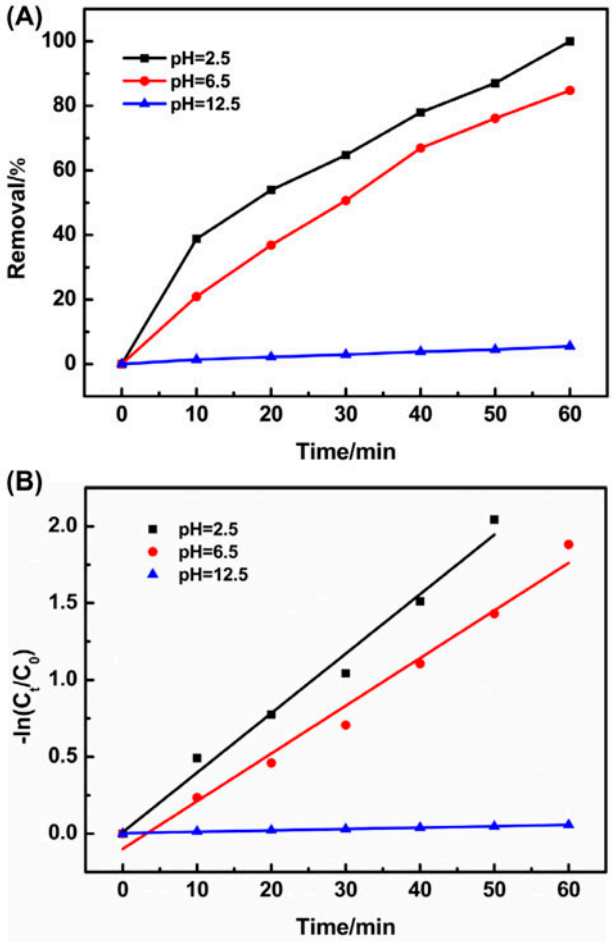

Fig. 7. Effect of pH on the photocatalytic reduction of Cr(VI) solution ([Cr(VI)] = 20 mg L^{-1}, ethanol as hole scavenger): (A) Removal efficiency of Cr(VI) and (B) plot of –ln (C_t/C_0) vs. time of Cr(VI).

Fig. 7(A) shows the reduction of Cr(VI) at different pH. Obviously, there is a vital influence of the variation of pH on the reduction of Cr(VI) to Cr(III). The photoreduction efficiency is higher when performed in acidic solutions than that in alkaline solutions. At pH 2.5, it showed a fast reduction with Cr(VI) reduction efficiency of 100% in 60 min. However, with the pH increasing, the efficiency decreased to 84.5 and 5.5% at pH 6.5 and 12.5.

The rate constants of photocatalytic reduction of Cr(VI) were calculated to be 0.0387, 0.0310 and 0.0009 min^{-1} for pH 2.5, 6.5, and 12.5, respectively. The effect of the varied pH was in accordance with previous studies [53]. Because the dominant chromium species is $Cr_2O_7^{2-}$ at low pH, the overall reduction reaction can be described as follows:

$$Cr_2O_7^{2-} + 14H^+ + 6e^- \leftrightharpoons 2Cr(III) + 7H_2O \quad (3)$$

According to the equation, the higher concentration of H^+ will result in Eq. (1), shifting to the right-hand side, which cause high Cr(VI) reduction efficiency. In addition, the reduction potential of chromium ions at low pH is more positive than that of the conduction band of TiO_2 [54].

3.3. Photoelectrochemical characterization and electron transfer mechanism investigation

The open-circuit photovoltage (V_{oc}) is considered as the accumulation of photogenerated charge transferring to TiO_2/electrolyte interface. As shown in Fig. 8, the photovoltage of $Cu_{0.01}/TiO_2$ NTs was

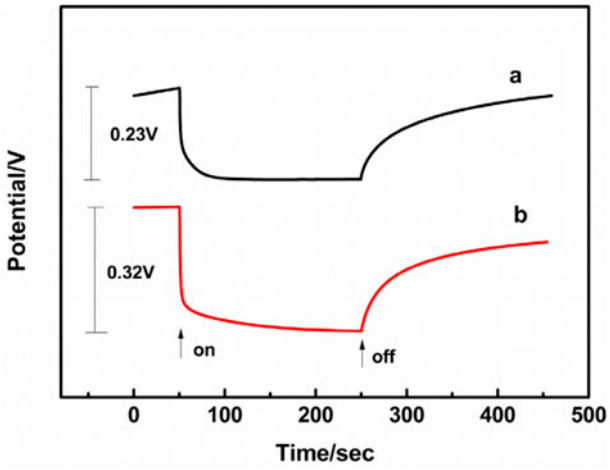

Fig. 8. The open-circuit photovoltage vs. time curves of (a) TiO_2 NTs and (b) $Cu_{0.01}/TiO_2$ NTs.

0.32 V, which was higher than that of unmodified TiO_2 for 0.23 V upon illumination. It indicated that there were more photogenerated electrons accumulated on the surface of the Cu/TiO_2 NTs. When stopping the illumination, the potential decayed slowly as the accumulated photoelectrons begin to leak out of the TiO_2 NTs to dissipate gradually. The $Cu_{0.01}/TiO_2$ NTs showed the slower decay, which was indicated a long lifetime of hole–electron pairs and a high photocatalytic activity during photoreaction. The result manifested that the Cu–TiO_2 Schottky barrier can prevent the recombination of the holes and electrons effectively.

EIS is an effective technique for evaluating the charge transfer and recombination processes at the contact interface between the electrode and electrolyte solution [55]. Fig. 9(A) displayed the EIS Nynquist plots of the pure TiO_2 NTs and $Cu_{0.01}/TiO_2$ NTs under dark and UV-light irradiation conditions. They were measured in aqueous 0.25 mol L^{-1} Na_2SO_4 solution using the amplitude of 5 mV at OCP. It can be seen clearly that the curve radii are both reduced with the UV-light irradiation on the pure TiO_2 NTs and $Cu_{0.01}/TiO_2$ NTs, which is due to the separation of photogenerated electrons and holes. Moreover, the curve radius of $Cu_{0.01}/TiO_2$ NTs was smaller than that of TiO_2 NTs either in dark or under UV-light irradiation. The results indicated that the Schottky barrier formed on Cu/TiO_2 NTs could improve the separation of photogenerated electron–hole pairs and decrease the charge transfer resistance, which lead to a fast interfacial transfer of electrons.

The Mott–Schottky plots of the potential range (−1.0 to 1.0 V) for the pure TiO_2 NTs and $Cu_{0.01}/TiO_2$

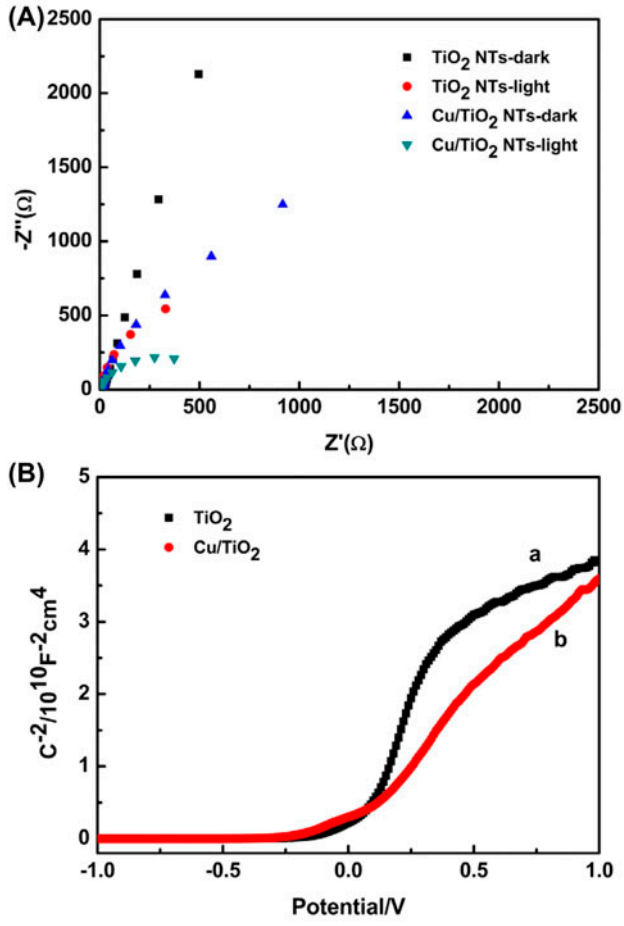

Fig. 9. (A) EIS response of TiO_2 NTs and $Cu_{0.01}/TiO_2$ NTs electrodes measured at OCP in the dark and under UV irradiation, respectively and (B) Mott–Schottky plots of: (a) TiO_2 NTs and (b) $Cu_{0.01}/TiO_2$ NTs electrodes at potential range of −1.0–1.0 V vs. SCE.

NTs under UV light are shown in Fig. 9(B). The Mott–Schottky plots can confirm the type of semiconductor and evaluate the electron-transfer of semiconductor interface. From Fig. 9(B), positive slopes could indicate that the photoelectrodes are n-type semiconductors. The capacitance C was related to the charge carrier density according to the following equation [55]:

$$\frac{1}{C^2} = \frac{2}{e\varepsilon\varepsilon_0 N_D}\left(E - E_{FB} - \frac{KT}{e}\right) \quad (4)$$

where e is the elementary electron charge, ε is the permittivity of the semiconductor, ε_0 is the permittivity of vacuum, N_D is the charge carrier density, E is the applied potential, E_{FB} is the flat band potential, k is the Boltzmann constant, and T is the temperature.

Meanwhile, the carrier density N_D could be calculated from the following equation:

$$N_D = \frac{2}{e\varepsilon\varepsilon_0 m} \quad (5)$$

where m is the slope of the Mott–Schottky plot, $e = 1.6 \times 10^{-19}$, $\varepsilon_0 = 8.86 \times 10^{-14}$ F cm^{-1}, and $\varepsilon = 80$ for TiO_2 [44]. Therefore, the charge carrier density of the pure TiO_2 NTs and Cu/TiO_2 NTs was estimated to be 1.39×10^{19} and 3.78×10^{19}, respectively. The higher N_D of Cu/TiO_2 NTs indicated a faster charge transfer on the interface of Cu and TiO_2, and an enhanced photocatalytic performance.

From the analysis above, the Cu/TiO_2 NTs exhibit enhanced photoelectrochemical properties and photocatalytic activity due to the uniform distribution of Cu particles with good stability. Thus, the principle of the electron and hole transferring on Cu/TiO_2 NTs is summarized in Fig. 10. TiO_2 is an n-type semiconductor with wide band gap (3.2 eV). When UV irradiation is used on the TiO_2 NTs, the photogenerated electrons will promptly transfer from its valence band to conduction band and leave the hole in valence band. However, the lifetime is very short and the electron–hole pairs will recombine rapidly. Since the Fermi level of metals such as Cu ($E_f = -4.7$ eV vs. vacuum level) is more negative than the conduction band of TiO_2, Cu particles can be regarded as receiving device for the photogenerated electrons that can transfer from the conduction band of TiO_2 to metal Cu after Cu is loaded on the TiO_2 NTs. Until the two Fermi levels are equal, the Cu particles get more electrons which almost disappear on the surface of TiO_2. At the same time, the band of TiO_2 bends up towards the surface to form a space charge layer called "carriers depleted" [56]. A Schottky barrier that forms on the interface of Cu and TiO_2 can make a good fluidity due to its diode property for accumulated electrons transferring from TiO_2 to Cu particles. The reduction from Cr(VI) to Cr(III) will occur by the electrons accumulated at Cu particles and holes accumulated in the valence band of the TiO_2 can react with H_2O or OH^- to form hydroxyl radicals ($OH^{\cdot}$). The processes can be depicted as following reaction (2)–(5):

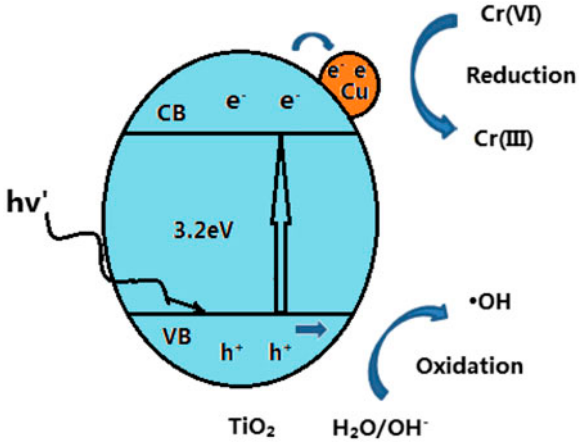

Fig. 10. Illustrative diagrams of the electron and hole transfer in Cu/TiO_2 NTs.

$$TiO_2 + h\nu \rightarrow TiO_2(e^-) + TiO_2(h^+) \quad (6)$$

$$TiO_2(e^-) + Cu \rightarrow TiO_2 + Cu(e^-) \quad (7)$$

$$Cr(VI) + 3e^- \rightarrow Cr(III) \quad (8)$$

$$TiO_2(h^+) + H_2O \rightarrow H^+ + OH^{\cdot} \quad (9)$$

The semiconductor–metal system can suppress the recombination of electrons and holes effectively and the photogenerated electron will continuously transfer from semiconductor to metal, resulting in efficient electron–hole separation and high photocatalytic activity.

4. Conclusions

The highly ordered TiO_2 NTs were fabricated by electrochemical anodic oxidation and Cu particles were loaded on the surface of TiO_2 NTs using an impregnation–reduction method. Compared with the unmodified TiO_2 NTs, the Cu/TiO_2 NTs showed a much higher photocatalytic reduction for Cr(VI). The maximum rate constant of photocatalytic reduction of Cr(VI) on $Cu_{0.01}$/TiO_2 NTs was 9.5 times higher than that on unmodified TiO_2 NTs. The Cu/TiO_2 NTs have enhanced photocurrent, more negative open-circuit voltage, and higher charge transfer rate. The results can be attributed to the Schottky barrier formed on the interface of Cu and TiO_2 which can improve the electron–hole separation and suppress the recombination. The high photocatalytic efficiency, low cost, and less pollution of Cu/TiO_2 NTs may have potential application in environmental remediation.

Supplementary material

The supplementary material for this paper is available online at http://dx.doi.10.1080/19443994.2015.1041052.

Acknowledgment

The project was supported by National Natural Science Foundation of China (No. 21,476,053, 51,179,033), the Doctoral Program of the Ministry of Education (No. 20,132,304,110,027), the Fundamental Research Funds for the Central Universities, and Special Fund Research Program for Talents of Science Technology Innovation in Harbin (No. 2009RFXXG204).

References

[1] Q. Wu, J. Zhao, G. Qin, C. Wang, X. Tong, S. Xue, Photocatalytic reduction of Cr(VI) with TiO_2 film under visible light, Appl. Catal. B. 142–143 (2013) 142–148.
[2] H. Chen, Y. Shao, Z. Xu, H. Wan, Y. Wan, S. Zheng, D. Zhu, Effective catalytic reduction of Cr(VI) over TiO_2 nanotube supported Pd catalysts, Appl. Catal. B. 105 (2011) 255–262.
[3] Y. Zhang, J. Li, M. Zhang, D.D. Dionysiou, Size-tunable hydrothermal synthesis of SnS_2 nanocrystals with high performance in visible light-driven photocatalytic reduction of aqueous Cr(VI), Environ. Sci. Technol. 45 (2011) 9324–9331.
[4] Y. Zhang, L. Yao, G. Zhang, D.D. Dionysiou, J. Li, X. Du, One-step hydrothermal synthesis of high-performance visible-light-driven SnS_2/SnO_2 nanoheterojunction photocatalyst for the reduction of aqueous Cr(VI), Appl. Catal. B. 144 (2014) 730–738.
[5] Y. Zhang, J. Li, H.Y. Xu, One-step *in-situ* solvothermal synthesis of SnS_2/TiO_2 nanocomposites with high performance in visible light-driven photocatalytic reduction of aqueous Cr(VI), Appl. Catal. B 123–124 (2012) 18–26.
[6] Z. Sun, L. Zheng, S. Zheng, R.L. Frost, Preparation and characterization of TiO_2/acid leached serpentinite tailings composites and their photocatalytic reduction of Chromium(VI), J. Colloid Interface Sci. 404 (2013) 102–109.
[7] M.R. Samarghandi, J.K. Yang, S.M. Lee, O. Giahi, M. Shirzad-Siboni, Effect of different type of organic compounds on the photocatalytic reduction of Cr(VI) in presence of ZnO nanoparticles, Desalin. Water Treat. 52 (2014) 1531–1538.
[8] X.F. Lei, X.X. Xue, H. Yang, Preparation and characterization of Ag-doped TiO_2 nanomaterials and their photocatalytic reduction of Cr(VI) under visible light, Appl. Surf. Sci. 321 (2014) 396–403.
[9] X. Liu, T. Lv, Y. Liu, L. Pan, Z. Sun, TiO_2–Au composite for efficient UV photocatalytic reduction of Cr(VI), Desalin. Water Treat. 51 (2013) 3889–3895.
[10] W. Yang, Y. Liu, Y. Hu, M. Zhou, H. Qian, Microwave-assisted synthesis of porous CdO–CdS core–shell nanoboxes with enhanced visible-light-driven photocatalytic reduction of Cr(vi), J. Mater. Chem. 22 (2012) 13895–13898.
[11] Y. Wang, W. Yang, L. Zhang, Y. Hu, X.W. (David) Lou, Formation of MS–Ag and MS (M = Pb, Cd, Zn) nanotubes via microwave-assisted cation exchange and their enhanced photocatalytic activities, Nanoscale 5 (2013) 10864–10867.
[12] X. Gao, H.B. Wu, L. Zheng, Y. Zhong, Y. Hu, X.W. Lou, Formation of Mesoporous Heterostructured $BiVO_4/Bi_2S_3$ Hollow Discoids with Enhanced Photoactivity, Angew. Chem. Int. Ed. 53 (2014) 5917–5921.
[13] K.M. Parida, N. Sahu, Visible light induced photocatalytic activity of rare earth titania nanocomposites, J. Mol. Catal. A: Chem. 287 (2008) 151–158.
[14] Dipti P. Das, K. Parida, B.R. De, Photocatalytic reduction of hexavalent chromium in aqueous solution over titania pillared zirconium phosphate and titanium phosphate under solar radiation, J. Mol. Catal. A: Chem. 245 (2006) 217–224.
[15] P. Mohapatra, S.K. Samantaray, K. Parida, Photocatalytic reduction of hexavalent chromium in aqueous solution over sulphate modified titania, J. Photochem. Photobiol. A. 170 (2005) 189–194.
[16] Y. Zhang, M. Yang, G. Zhang, D.D. Dionysiou, HNO_3-involved one-step low temperature solvothermal synthesis of N-doped TiO_2 nanocrystals for efficient photocatalytic reduction of Cr(VI) in water, Appl. Catal. B. 142–143 (2013) 249–258.
[17] M. Pelaez, N.T. Nolan, S.C. Pillai, M.K. Seery, P. Falaras, A.G. Kontos, P.S.M. Dunlop, J.W.J. Hamilton, J.A. Byrne, K. O'Shea, M.H. Entezari, D.D. Dionysiou, A review on the visible light active titanium dioxide photocatalysts for environmental, Appl. Catal. B. 125 (2012) 331–349.
[18] L.G. Devi, R. Kavitha, A review on non metal ion doped titania for the photocatalytic degradation of organic pollutants under UV/solar light: Role of photogenerated charge carrier dynamics in enhancing the activity, Appl. Catal. B. 140–141 (2013) 559–587.
[19] Q. Wang, X. Yang, D. Liu, L. Chi, J. Hou, Ag and CdS nanoparticles co-sensitized TiO_2 nanotubes for enhancing visible photoelectrochemical performance, Electrochim. Acta. 83 (2012) 140–145.
[20] X. Zhang, Y. Tang, Y. Li, Y. Wang, X. Liu, C. Liu, S. Luo, Reduced graphene oxide and PbS nanoparticles co-modified TiO_2 nanotube arrays as a recyclable and stable photocatalyst for efficient degradation of pentachlorophenol, Appl. Catal. A. 457 (2013) 78–84.
[21] F. Cai, F. Yang, J. Xi, Y. Jia, C. Cheng, Y. Zhao, Ultrasound effect: Preparation of PbS/TiO_2 heterostructure nanotube arrays through successive ionic layer adsorption and the reaction method, Mater. Lett. 107 (2013) 39–41.
[22] L. Liu, J. Lv, G.Q. Xu, Y. Wang, K. Xie, Z. Chen, Y. Wu, Uniformly dispersed CdS nanoparticles sensitized TiO_2 nanotube arrays with enhanced visible-light photocatalytic activity and stability, J. Solid State Chem. 208 (2013) 27–34.
[23] G. Song, F. Xin, J. Chen, X. Yin, Photocatalytic reduction of CO_2 in cyclohexanol on CdS–TiO_2 heterostructured photocatalyst, Appl. Catal. A. 473 (2014) 90–95.
[24] X. Liu, L. Pan, T. Lv, Z. Sun, CdS sensitized TiO_2 film for photocatalytic reduction of Cr(VI) by microwave-assisted chemical bath deposition method, J. Alloys Compd. 583 (2014) 390–395.
[25] L. Yang, W. Sun, S. Luo, Y. Luo, White fungus-like mesoporous Bi_2S_3 ball/TiO_2 heterojunction with high photocatalytic efficiency in purifying 2,4-dichlorophenoxyacetic acid/Cr(VI) contaminated water, Appl. Catal., B. 156–157 (2014) 25–34.

[26] X. Zhao, H. Liu, J. Qu, Photoelectrocatalytic degradation of organic contaminants at Bi_2O_3/TiO_2 nanotube array electrode, Appl. Surf. Sci. 257 (2011) 4621–4624.
[27] H. Liu, H. Shon, X. Sun, S. Vigneswaran, H. Nan, Preparation and characterization of visible light responsive Fe_2O_3–TiO_2 composites, Appl. Surf. Sci. 257 (2011) 5813–5819.
[28] S. Kuang, L. Yang, S. Luo, Q. Cai, Fabrication, characterization and photoelectrochemical properties of Fe_2O_3 modified TiO_2 nanotube arrays, Appl. Surf. Sci. 255 (2009) 7385–7388.
[29] L. Yang, S. Luo, Y. Li, Y. Xiao, Q. Kang, Q. Cai, High efficient photocatalytic degradation of p-nitrophenol on a unique Cu_2O/TiO_2 p–n heterojunction network catalyst, Environ. Sci. Technol. 44 (2010) 7641–7646.
[30] Y. Hou, X. Li, X. Zou, X. Quan, G. Chen, Photoeletrocatalytic activity of a Cu_2O-loaded self-organized highly oriented TiO_2 nanotube array electrode for 4-chlorophenol degradation, Environ. Sci. Technol. 43 (2009) 858–863.
[31] L. Assaud, V. Heresanu, M. Hanbücken, L. Santinacci, Fabrication of p/n heterojunctions by electrochemical deposition of Cu_2O onto TiO_2 nanotubes, C. R. Chim. 16 (2013) 89–95.
[32] J. Ma, M. Yang, Y. Sun, C. Li, Q. Li, F. Gao, F. Yu, J. Chen, Fabrication of Ag/TiO_2 nanotube array with enhanced photo-catalytic degradation of aqueous organic pollutant, Physica E. 58 (2014) 24–29.
[33] Y. Jiang, B. Zheng, J. Du, G. Liu, Y. Guo, D. Xiao, Electrophoresis deposition of Ag nanoparticles on TiO_2 nanotube arrays electrode for hydrogen peroxide sensing, Talanta 112 (2013) 129–135.
[34] G. Guo, B. Yu, P. Yu, X. Chen, Synthesis and photocatalytic applications of Ag/TiO_2-nanotubes, Talanta 79 (2009) 570–575.
[35] X. Pang, D. He, S. Luo, Q. Cai, An amperometric glucose biosensor fabricated with Pt nanoparticle-decorated carbon nanotubes/TiO_2 nanotube arrays composite, Sens. Actuators B. 137 (2009) 134–138.
[36] M. Hosseini, M.M. Momeni, Gold particles supported on self-organized nanotubular TiO_2 matrix as highly active catalysts for electrochemical oxidation of glucose, J Solid State Electrochem. 14 (2010) 1109–1115.
[37] A. Takai, P.V. Kamat, Capture, store, and discharge. Shuttling photogenerated electrons across TiO_2–silver interface, ACS Nano. 5 (2011) 7369–7376.
[38] P. Xiao, L. Li, Y. Zhang, H. Dai, Y. Hu, L. Lu, Enhanced photoelectrochemical property of Zn loaded TiO_2 nanotube arrays electrode, Chin. J. Chem. Phys. 23 (2010) 113–116.
[39] G.K. Parshetti, R.A. Doong, Synergistic effect of nickel ions on the coupled dechlorination of trichloroethylene and 2,4-dichlorophenol by Fe/TiO_2 nanocomposites in the presence of UV light under anoxic conditions, Water Res. 45 (2011) 4198–4210.
[40] Y. Liu, Z. Wang, W. Fan, Z. Geng, L. Feng, Enhancement of the photocatalytic performance of Ni-loaded TiO_2 photocatalyst under sunlight, Ceram. Int. 40 (2014) 3887–3893.
[41] H.J. Kim, L.H. Lu, J.H. Kim, C.H. Lee, T.W. Hyeon, W.Y. Choi, H.I. Lee, UV light induced photocatalytic degradation of cyanides in aqueous solution over modified TiO_2, Bull. Korean Chem. Soc. 22 (2001) 1371–1374.
[42] T.D. Pham, B.K. Lee, Cu doped TiO_2/GF for photocatalytic disinfection of *Escherichia coli* in bioaerosols under visible light irradiation: Application and mechanism, Appl. Surf. Sci. 296 (2014) 15–23.
[43] X. Cheng, H. Liu, Q. Chen, J. Li, P. Wang, Preparation and characterization of palladium nano-crystallite decorated TiO_2 nano-tubes photoelectrode and its enhanced photocatalytic efficiency for degradation of diclofenac, J. Hazard. Mater. 254–255 (2013) 141–148.
[44] S. Luo, Y. Xiao, L. Yang, C. Liu, F. Su, Y. Li, Q. Cai, G. Zeng, Simultaneous detoxification of hexavalent chromium and acid orange 7 by a novel Au/TiO_2 heterojunction composite nanotube arrays, Sep. Purif. Technol. 79 (2011) 85–91.
[45] Z. Li, J. Liu, D. Wang, Y. Gao, J. Shen, $Cu_2O/Cu/TiO_2$ nanotube Ohmic heterojunction arrays with enhanced photocatalytic hydrogen production activity, Int. J. Hydrogen Energy. 37 (2012) 6431–6437.
[46] Y. Chen, D.D. Dionysiou, A comparative study on physicochemical properties and photocatalytic behavior of macroporous TiO_2-P25 composite films and macroporous TiO_2 films coated on stainless steel substrate, Appl. Catal. A. 317 (2007) 129–137.
[47] W. Li, M. Chen, Synthesis of stable ultra-small Cu nanoparticles for direct writing flexible electronics, Appl. Surf. Sci. 290 (2014) 240–245.
[48] D. Wang, B. Yu, F. Zhou, C. Wang, W. Liu, Synthesis and characterization of anatase TiO_2 nanotubes and their use in dye-sensitized solar cells, Mater. Chem. Phys. 113 (2009) 602–606.
[49] H. Li, C. Guo, C. Xu, A highly sensitive non-enzymatic glucose sensor based on bimetallic Cu–Ag superstructures, Biosens. Bioelectron. 63 (2015) 339–346.
[50] F. Alonso, T. Melkonian, Y. Moglie, M. Yus, Homocoupling of terminal alkynes catalysed by ultrafine copper nanoparticles on titania, Eur. J. Org. Chem. 13 (2011) 2524–2530.
[51] G.K. Mor, K. Shankar, M. Paulose, O.K. Varghese, C.A. Grimes, Enhanced photocleavage of water using titania nanotube arrays, Nano Lett. 5 (2005) 191–195.
[52] Q. Wang, X. Yang, D. Liu, J. Zhao, Fabrication, characterization and photocatalytic properties of Ag nanoparticles modified TiO_2 NTs, J. Alloys Compd. 527 (2012) 106–111.
[53] L. Yang, Y. Xiao, S. Liu, Y. Li, Q. Cai, S. Luo, G. Zeng, Photocatalytic reduction of Cr(VI) on WO_3 doped long TiO_2 nanotube arrays in the presence of citric acid, Appl. Catal. B 94 (2010) 142–149.
[54] J.Y. Yoon, E.J. Shim, S.Y. Bae, H.K. Joo, Application of immobilized nanotubular TiO_2 electrode for photocatalytic hydrogen evolution: Reduction of hexavalent chromium (Cr(VI)) in water, J. Hazard. Mater. 161 (2009) 1069–1074.
[55] T. Li, X. Li, Q. Zhao, Y. Shi, W. Teng, Fabrication of n-type $CuInS_2$ modified TiO_2 nanotube arrays heterostructure photoelectrode with enhanced photoelectrocatalytic properties, Appl. Catal. B. 156–157 (2014) 362–370.
[56] Q. Kang, Q. Lu, S. Liu, L. Yang, L. Wen, S. Luo, Q. Cai, A ternary hybrid CdS/Pt–TiO_2 nanotube structure for photoelectrocatalytic bactericidal effects on *Escherichia coli*, Biomaterials 31 (2010) 3317–3326.